Applied Mathematics and Computation 246 (2014) 440–446

Contents lists available at ScienceDirect

Applied Mathematics and Computation

journal homepage: www.elsevier.com/locate/amc

Unified QLM for regular and arbitrary singular potentials

R. Krivec

Department of Theoretical Physics, J. Stefan Institute, Jamova 39, 1000 Ljubljana, Slovenia

ARTICLE INFO

Keywords:
Quasilinearization
Singular potentials
Spiked oscillator
Exponentially spiked oscillator
Nonlinear perturbation theory
Klauder effect

ABSTRACT

A parameterless numerical implementation of the Quasilinearization Method (QLM) is constructed and tested to 21–25 digits precision to give quadratically convergent energies E of the Klauder effect exhibiting spiked harmonic oscillator with the λ/r^α or $\exp(\lambda/r^\alpha)$ type spikes in a Riccati reformulation of the Schrödinger equation. The radial solution is uniformly quadratic convergent to the same precision as E, except in the small minorization interval where the self-correcting property of QLM assures geometric convergence like in the Picard algorithm to about 12–16 digits, sufficient not to affect the convergence of E, confirming what is expected on physical grounds. It was shown before that for regular potentials, immediate onset of quadratic convergence is guaranteed by the initial iteration of the WKB form, and that for quadratic convergence of E for power-type spikes it suffices to augment this by a nonlinear integration point distribution and by minorization of (negative) solution values. The form of the Riccati equation used allows the minorization function to easily be formally defined over the entire interval, without the need for a cutoff radius of application, and dependence on its scale factor is plateau-like and negligible.

1. Introduction

For decades [1] a general method of solution has been sought applicable to small and large values $\lambda,\ \alpha$ for the spiked harmonic oscillator (SHO) potential,

$$V = r^2 + \frac{\lambda}{r^\alpha}. \tag{1}$$

Potentials of this type appear in molecular, atomic, nuclear and particle physics, for example in scattering [3,4], As Klauder has shown [5–10], the effect of the spike does not vanish in the limit $\lambda \to 0$. Detwiler and Klauder [5] have also shown that its matrix elements diverge (supersingularity for $\alpha \geqslant 5/2$), and the WKB method cannot be used. Analytical and numerical approaches limited to small regions of the $\lambda,\ \alpha$ space have been used to calculate energies and wave functions of SHO starting with variational and large-coupling perturbative expansions by [1], followed by e.g. [11] and culminating with Ref. [12], which is an algebraic method for a finite sum of λ/r^α type spikes.

A purely numerical approach has rarely been pursued, e.g. in [13], and such approaches relied on the detailed form of the singular terms. However, from the viewpoint of QLM, a purely numerical approach is worth trying, as the "self-correcting' property of OLM iterations might maintain convergence near singularities. In the work [2], QLM [14] has been applied to the SHO using an "adaptive grid" and a minorization technique to regularize effects of numerical errors, resulting in E values with up to 28 digits precision for a large region of $\alpha,\ \lambda$ values. In the present work we modify, automatize algorithms

E-mail address: rajmund.krivec@ijs.si

http://dx.doi.org/10.1016/j.amc.2014.08.051
0096-3003/

and test the independence of our method of the form of V by applying it to a very singular infinite series version of the potential in Ref. [12], and analyze local convergence of the radial solution in comparison with earlier applications to different potentials.

2. The QLM approach

The QLM devised by Mandelzweig [15] is a generalization of an iterative method for solving nonlinear differential equations to arbitrary regular and singular potentials, able of quadratic and often monotonic convergence [16]. It is applied in quantum mechanics by rewriting the radial Schrödinger equation as a Riccati equation for a function expressed in terms of the logarithmic derivative $\phi(r)$ of the wave function. QLM is a resummation of WKB: the kth QLM iteration sums 2^k terms [17,18] of the WKB series. For exactly solvable potentials the first QLM iteration gives exact energies if a quantization condition is imposed [19]. Quadratic convergence starts once the norm of the difference of the current and previous iterations is small enough [15].

However, a practical numerical implementation of QLM requires (i) a method to control the onset of quadratic convergence, i.e., to guarantee its onset already at the first iteration, and (ii) a method to handle singular points preferably without changing the form of equations, i.e., without coordinate transformations.

Our numerical implementation for the radial Schrödinger equation [14,17,18,21], for easier handling of nodes in the radial solution $\chi(r)$, uses the (negative) form of solution:

$$u(x) = \arctan\left(-\frac{\kappa}{\phi(r)}\right) = \arctan\left(-\kappa\frac{\chi(r)}{\chi'(r)}\right), \tag{2}$$

where $x = \kappa r,\ \kappa = \sqrt{E}$ with $2m = 1$. In the resulting Riccati equation

$$u'(x) = -1 + W\sin^2 u(x) = q(x, u(x)), \quad E > 0, \tag{3}$$

$W(x) = 2mV(r)/\kappa^2$ for angular momentum $l = 0$. The QLM iteration equations in differential form [14,21] for $k = 1, 2, \ldots, M$ are

$$u_k'(x) = q(x, u_{k-1}(x)) + (u_k(x) - u_{k-1}(x))q_u(x, u_{k-1}(x)) = Q(x, u_{k-1}(x), u_k(x)), \tag{4}$$

or, in simplified notation,

$$Q(x, u_{k-1}, u_k) = -1 + W\sin^2 u_{k-1} + (u_k - u_{k-1})W\sin 2u_{k-1} \tag{5}$$

with q_u denoting the functional derivative $\partial q(x, u(x))/\partial u$.

For regular potentials, the numerical implementation has been completed in the work [18], where the Langer WKB solution [20] was found to assure immediate onset of quadratic convergence of the QLM iteration.

For power-type singular potentials (exhibiting the Klauder effect), numerical noise due to large $W(x)$ but small $u^2(x)$ in products of the type $W(x)u(x)^2$ in Eq. (5) near the singularity may preclude the onset of quadratic convergence just like a bad initial solution does, as follows. The Klauder effect amounts to the fact that $q(0, u(0)) = Q(0, u_{k-1}(0), u_k(0)) = 0$ in Eqs. (4) and (5). (For regular potentials, $q(0, u(0)) = Q(0, u_{k-1}(0), u_k(0)) = -1$.) We must ensure that numerically the terms of $Q(x, u_{k-1}, u_k)$ cancel out near the origin. The work [2] demonstrated that to guarantee immediate onset of quadratic convergence, it is sufficient to (i) construct a special "adaptive grid" point distribution not unlike the approach taken in the Finite Element Method, and (ii) simply confine (minorize) the numerical noise of $u(x) \leqslant 0$ near the origin into a finite interval provided by a small multiplier of the leading term of the solution near the origin. This works well as long as large values of $W(x)$ are representable in the computer sufficiently close to the singularities.

The goal of the present work is (a) to improve the automatic algorithm for point density (which was not entirely automatic in [2]), (b) to address the problem of computer representability of large $V(r)$ or $W(x)$ values near the singularities, and (c) to check for local deviations from quadratic convergence of $u(x)$ due to minorization and their effect on convergence of E. The aim is a unified QLM numerical implementation to give stable results for both regular and singular potentials without resorting for example to coordinate transformations which may not be suitable across the whole LHS subinterval in the matching procedure. To this end we chose the exponentially spiked harmonic oscillator potential (ESHO),

$$V = r^2 + \mu e^{\lambda r^{-\alpha}}, \tag{6}$$

which can be viewed as a series of power-law spike terms $(\lambda^k/k!)r^{-k\alpha},\ k = 1, \ldots, \infty$ like in Eq. (1), or a generalization of the finite-sum potential of Ref. [12], or representing a special case of nonlinear perturbation [22]. We expect ESHO will exceed all the difficulties of the SHO. Supersingular potentials of the form $\exp(\lambda r^{-\beta})r^{-m}$ were studied before in works on the so-called "peratization" method of regularization [4,23,24]. The potential Eq. (6) and the corresponding potential with the singularity at infinity are representatives of the class of potentials dealt with in [5].

3. Behavior near the singularity

Near the origin a representation of the ESHO solution to leading order is

$$\tilde{\chi}(r) \approx \exp\left(-ar^{\alpha+1}e^{\frac{\lambda}{2}r^{-\alpha}}\right) \tag{7}$$

or

$$\tilde{u}(x) \approx -\frac{\kappa}{\sqrt{2m\mu}}e^{-\frac{\lambda}{2}\left(\frac{x}{\kappa}\right)^{-\alpha}}, \tag{8}$$

where $a = 2\sqrt{2m\mu}/\alpha\lambda$. (The tangent function is omitted in Eq. (8) [2]).

4. Numerical approach

4.1. Representability near the singularity

If the largest positive machine-representable number at given precision is 2^η, and its natural logarithm is e_η, the minimum r for evaluating V of Eq. (6) is

$$r_\eta \approx \left(\frac{\lambda}{e_\eta - \log\mu}\right)^{\frac{1}{\alpha}}. \tag{9}$$

For example, for $\mu = 1,\ \lambda = 0.0001,\ \alpha = 2.5$, and $\eta = 16383$ for 128-bit representation, we have $e_\eta \approx 11356$ and $r_\eta \approx 0.0006$, which is too large for obtaining large precision.

We modified parts of the code that evaluate expressions like $W(x)\sin^2 u(x)$ (Eq. (5)) to now optionally use $\log|W(x)|$ instead of $W(x)$, and the V-evaluating routines to return $\log|V(r)|$ instead of $V(r)$. $u(x)$ code is unchanged. If logarithmic representation is used, r_η is not used as lower limit on r, since it would be very difficult to reach the representation limit.

The effect of logarithmic representation on accuracy is weak. In computer representation of a floating-point number p with fixed-length mantissa, $\Delta p/p \approx \epsilon$, where ϵ is a machine constant. In 128-bit floating-point precision, it is typically $2^{-112} \approx 10^{-33}$. If $p = \log V,\ \Delta p/p = (\Delta V/V)/\log V \approx \epsilon$, or $\Delta V/V \approx \epsilon \log V$.

It is not necessary to apply the above procedures to the initial QLM approximation, i.e. the Langer WKB solution. It can be set to 0 for $x < \kappa r_\eta$ where V is not numerically representable. This is a similar situation as appears at the boundary x of the LHS and RHS Langer WKB functions [18], where the Langer solution has a step but already the first QLM iteration $u_{1(x)}$ is smooth. Thus unchanged WKB part of code can be used.

4.2. Point density

The nonlinear distribution $B_1 = \{x_i\}$ of N integration points on the LHS of the matching point x_m is a generalized implementation of the distribution "B" used in [2]. If $\{z_i\} = \{0,\ldots,z_N\}$ is an equidistant set, $\{x_i\}$ are defined right-to-left using the form $\tilde{\chi}(r)$ of Eq. (7) scaled by a factor A so that the resulting distribution inflection point always coincides with x_m

$$x_i = A\exp\left(-az_i^{\alpha+1}e^{\frac{\lambda}{2}z_i^{-\alpha}}\right). \tag{10}$$

(Previously [2] the inflection point was not moved to x_m which caused the algorithm breakdown in some cases.) We take $A = 1$ and detect the inflection point by searching for largest point separation on $(0, z_N = x_m/\kappa)$. If no maximum is found, z_N is retained, otherwise it is redefined as the discovered inflection point. Since there is no simple a priori check for point sequence monotonicity, the above process is repeated until such distribution is achieved, or else a linear sequence is returned. Like in [2], if a number of points near the singularity are spaced by less than $10^{-\sigma_x}$, they are replaced by a linear distribution, which still reduces the final minimum separation below $10^{-\sigma_x}$ only as $O(N^{-1})$. The difference with respect to [2] is that if V is evaluated directly, σ_x is not an arbitrary parameter but is constrained by the V representability limit κr_η. However if $\log|V|$ is evaluated instead of V, then for all practical purposes σ_x is a free parameter in the sense of [2].

Tests have shown this point distribution to be in general increasingly more efficient with increasing requested precision than the coordinate transformation of [13] which results in linearly increasing point spacing.

4.3. Error regularization

Local convergence near a singularity is maintained by the minorization regularization ("UQ" of the work [2]): if $u_k(x) < f_m(x)$ (larger in absolute value), it is replaced by $f_m(x)$, if $u_k(x) > 0$, it is replaced by 0. Likewise $Q(x, u_{k-1}, u_k)$ is "clamped" to $[f'_m(x), 0]$.

For x smaller than a certain small value x_0 depending on the goodness of Eq. (7) the minorization function for $u(x)$ is

$$f_m(x) = F_m\tilde{u}(x), \quad x \leqslant x_0, \tag{11}$$

where $\tilde{u}$ is given by Eq. (8), and F_m is an arbitrary multiplication parameter. In the course of the calculation, it is not possible to decide at which $x = x_0\, f_m(x)$ is no longer required, as we are comparing it with noisy $u(x)$ values; therefore f_m must be defined for all x, i.e., must be everywhere smaller than the (negative) correct solution. This is achieved by defining x_0 as the inflection point $x_0 : \tilde{u}''(x_0) = 0$:

$$x_0 = \left(\frac{\lambda\alpha\kappa^{\alpha}}{2(\alpha+1)}\right)^{\frac{1}{\alpha}} \tag{12}$$

and replacing Eq. (11) by a matched linearly extrapolated function (tangent to $\tilde{u}(x)$ at $x = x_0$) for $x > x_0$:

$$f_m(x) = F_m(\tilde{u}(x_0) + (x - x_0)\tilde{u}'(x_0)), \quad x > x_0. \tag{13}$$

Omitting the tangent function in Eq. (8) makes x_0 larger.

The crossover point x_c of a numerical iteration $u_k(x)$ and $f_m(x)$, like in [2], depends on numerical errors and the "external" parameter F_m; this ambiguity is again resolved by performing computations with several fixed values of F_m. If the dependence on F_m has a plateau [2] in a large interval whose lower border is close to 1, we consider the method stable and free from a regularization radius parameter.

4.4. Description of calculation

The approximate E values are first determined by a tabulation of the difference of the RHS and LHS solutions at the matching point $D(\kappa) = u_{M,\mathrm{LHS}}(x_m) - u_{M,\mathrm{RHS}}(x_m)$ [2].

The calculation proceeds automatically as in [2]: Eq. (4) is solved in two phases for different "external" parameters like F_m and σ_x using the algorithm B_1UQ. In the first phase the parameters are optimized for κ fixed close to the true κ and the "internal" parameters N, M, and x_u are gradually increased from some initial values N_0, M_0 and x_{u0} according to an optimization algorithm until $|D|$ is small enough. In each optimization pass the QLM iteration, starting with the lower precision initial Langer WKB solution, is performed. In the second phase we solve $D(\kappa) = 0$.

Like in [2], integration in this work has been performed using the fourth order explicit Runge–Kutta method with fifth order midpoint interpolation of $u_{k-1}(x)$ (Eq. (4)), so that integration error is clearly separated from QLM iteration error. 128-bit floating-point representation has been used.

5. Results

5.1. Convergence of $u(x)$ compared with SHO and regular potentials

Table 1 presents the convergence of QLM iterations in the linear metric (infinity norm, or maximum absolute difference over integration points $\{x_i\}$). For the regular Woods-Saxon potential, quadratic convergence is evident both for the infinite norm and for the LHS values of $u_k(x_m)$.

Table 1
QLM wave function convergence for regular and singular potentials. The first column for each potential displays logarithms of the infinity norm $\eta_{k\infty} = \log_{10}||u_k - u_{k-1}||_\infty$ (maximum value over the interval) of the absolute differences of successive QLM iterations $u_k(x)$ on the LHS; the corresponding second column displays logarithms of local absolute differences at the matching point, $\epsilon_k = \log_{10}|u_k(x_m) - u_{k-1}(x_m)|$. ϵ_k indicates both the uniform accuracy across points not close to singularity as well as accuracy of E, and exhibits quadratic convergence. For the Woods-Saxon potential, both $\eta_{k\infty}$ and ϵ_k exhibit quadratic convergence, i.e., doubling of precision on each iteration. For SHO [2], $\eta_{k\infty}$ converges quadratically only in the beginning, before the effects of the minorization take over ($\epsilon_k = -32$ indicates that convergence is limited by number representation and precise ϵ_k values are meaningless.) Similar results are obtained for the exponentially spiked oscillator (ESHO), calculated in the logarithmic representation of V; the largest x where minorization algorithm was triggered is 4×10^{-6} in the first case and 0.089 in the second case. ESHO demonstrates how QLM continues to improve local error for some time with geometric convergence.

k	Woods-Saxon [18]		SHO $\alpha = 2.5$, $\lambda = 0.0001$		ESHO $\alpha = 1$, $\lambda = 0.0001$		ESHO $\alpha = 1$, $\lambda = 1$	
	$\eta_{k\infty}$	ϵ_k	$\eta_{k\infty}$	ϵ_k	$\eta_{k\infty}$	ϵ_k	$\eta_{k\infty}$	ϵ_k
1		−1.20		−1.24		−2.24		−1.68
2	−2.79	−2.79	−4.07	−4.07	−4.96	−5.01	−3.45	−3.78
3	−6.51	−6.51	−10.10	−10.10	−9.78	−11.69	−5.10	−7.68
4	−14.32	−14.32	−19.37	−22.50	−10.41	−20.59	−5.73	−15.81
5	−30.30	−30.30	−18.67	−31.98	−11.59	−30.10	−6.94	−27.60
6			−18.69	−32	−12.86	−32	−9.34	−32
7			−18.57	−32	−14.97	−32	−11.96	−32
8			−18.96	−32	−16.72	−32	−13.48	−32
9					−16.36	−32	−13.25	−32
10					−16.35	−32	−12.96	−32
11					−16.68	−32	−9.37	−32
12					−16.35	−32	−11.67	−32

For singular potentials, regularization by minorization causes the solution near the singularity (at the origin) to converge slower in a small interval $[0, x_c]$ on which the minorization algorithm is "clamping" values, where the crossover point x_c is not prescribed in advance. In $[0, x_c]$ the convergence is geometric (linear) like in the Picard iteration algorithm [16]. In the case of the spiked oscillator potential [2] in Table 1, the infinity norm converges quadratically only in the beginning, before becoming limited by the local convergence in the minorization region. On the other hand, $u_k(x)$ outside of this region are not affected by the minorization procedure and converge quadratically.

Results are similar for the ESHO; difference in convergence is more pronounced with larger λ; the pointwise convergence in this case is displayed in Fig. 1, where relatively large values (of the order of 10^{-16}) appear on the relatively large interval (0, 0.089). However, the values are only about 2 orders of magnitude larger than for $\lambda = 0.0001$ (last part of Table 1).

Obviously integration precision is independent of, but must match the precision of the QLM iteration. As the Runge–Kutta integration has error $\approx O(N^{-4})$, we need roughly of the order of 10^5 points for 20 digit precision, etc. This is automatically provided by the code which repeats the QLM iteration with increasing N as well as increasing M until desired precision is reached. Fast convergence in m in most cases allows M to be fixed and intentionally rather large (as evident a posteriori) in order to save on the M optimization time.

It should be noted that if instead of minorization, $u_{k-1}(x)$ in Eq. (4) were joined at some $x = x_j$ with a truncated expansion like Eq. (7), we would not only acquire another parameter (x_j, presumably of the order of x_c) but would have no way of estimating the total error (numerical plus the error of the expansion) on $(0, x_j)$.

5.2. Convergence of E

Table 2 presents E values rounded to the number of stable digits, which may be slightly larger than the precision P requested from the parameter optimization algorithm. Up to 25 significant digits are displayed; this is nearly as much as

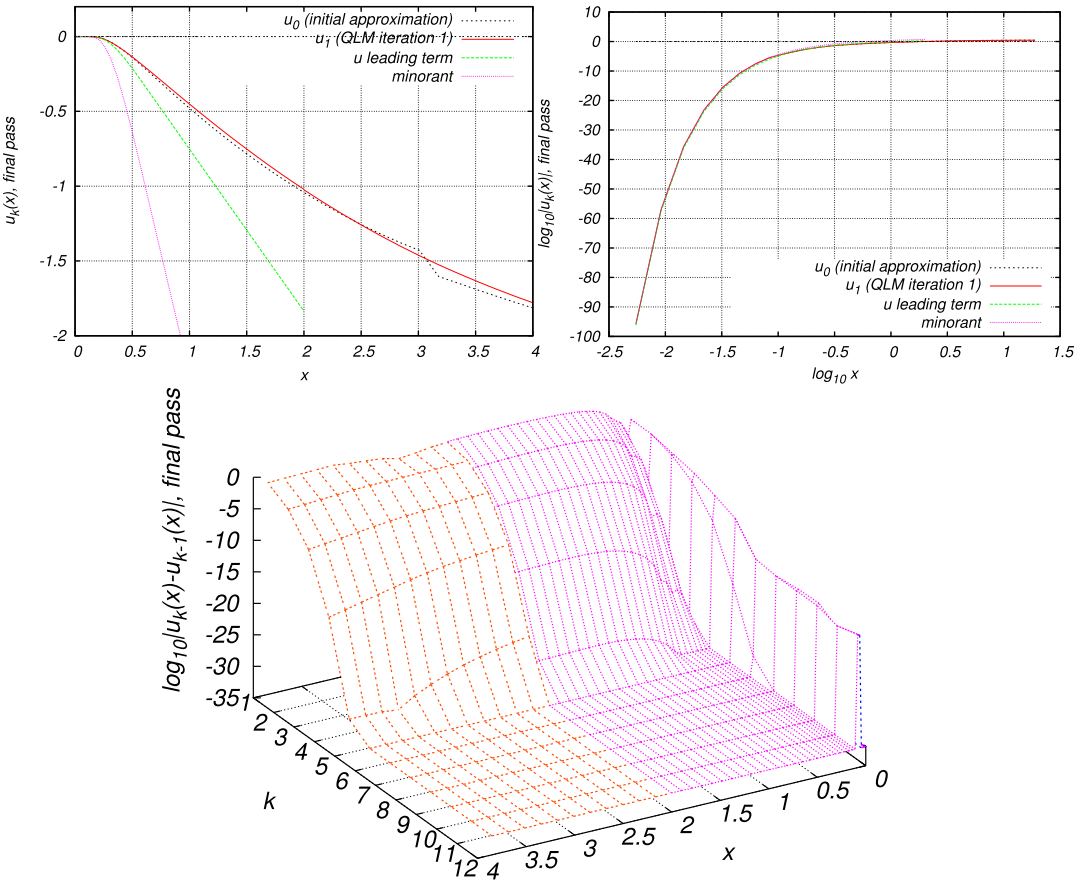

Fig. 1. QLM iterations of the radial solution and their absolute differences for small x ($x < 4$, $x_m = 2$) for the worst case of Table 1 (α=1, λ=1). Top left: iterations in linear scale. The initial Langer WKB iteration exhibits a step at $x \approx 3.1$ [18] (appearing extended due to plotting resolution), which is immediately removed by QLM iteration 1; higher QLM iterations are already indistinguishable from iteration 1 on the plot. Also shown are the leading term solution $\bar{u}$ and the minorant f_m for $F_m = 3$. Top right: same but showing logarithms of absolute values on both axes. Bottom: differences of successive QLM iterations $k = 1, \ldots, 12$. In the small minorization interval they exhibit geometric convergence and remain of the order of 10^{-12} but for all other x they converge uniformly quadratically (together with E) in just a few iterations before hitting the number representation limit.

Table 2
Energies for ESHO for $\mu = 1$ and different α, λ.

λ	α	P	x_m	x_m	M	N	E	$E - E_{\mathrm{SHO}}$
0.0001	1	20	1.0	15.08	8	2971101	4.000 120 209 493 762 545 13	
	2.5	24	1.5	16.32	8	126208903	4.019 500 484 397 453 880 862 195	1.019 093
	7	16	2.0	14.49	12	3635160	4.468 981 860 644 389 330 84	1.222 718
1	1	20	2.0	18.85	8	606131	5.947 670 144 334 628 741 43	
		24	2.0	20.40	8	5300000	5.947 670 144 334 628 741 432 474	
	2.5	20	3.0	19.61	12	2411282	6.081 340 849 816 087 358 93	1.764 029
	7	20	4.0	28.27	12	18117990	6.330 867 660 859 813 905 92	1.602 852

possible because we are close to the limit of the 128-bit arithmetic but do lose some precision via the logarithmic representation.

From Fig. 1 it is obvious that even in our extreme singular example, precision of the order of 20 digits in E is achieved with only four QLM iterations, like in previous work [2,14]. Because of this, we again usually fix M to values $4, 8, 12, \ldots$ and perform separate computations using different M, thus eliminating one convergence parameter.

For runs in Table 2 several control runs with one of the "internal" parameters larger than usual were made, like in SHO [2]. F_m is taken equal to 2 and 3, for which results agree to at least one more digit than the requested precision P. To verify this in more detail, the convergence for $\lambda = 1,\ \alpha = 1$ has been tested also for all combinations of $F_m = 1.0,\ 1.2,\ 1.5,\ 2.0,\ 3.0$ and $\sigma_x = 32,\ -64,\ -128,\ -160$. For the prescribed accuracy $P = 20$ we get 23 stable digits ($E = 5.\ldots 741\ 429\ 8$), with 21 correct as shown by the results for $P = 24$ where we get 26 stable digits ($E = 5.\ldots 741\ 432\ 473\ 7$). The test confirms the rule that we get $P + 1$ correct digits, therefore all values in Table 2 are rounded accordingly.

ESHO energies are shifted with respect to SHO (last column of Table 2).

5.3. Summary

The generalized minorization algorithm B_1UQ with logarithmic representation of V and the Runge–Kutta integration works for different α and large spans of λ, requiring roughly the same N as SHO. The precise value of the parameter F_m is unimportant, as is the value of σ_x, making the approach effectively parameterless like its precursor [2].

In the minorization intervals, the self-correcting nature of the QLM iteration equations still provides geometric (linear) convergence, which reached 12–16 digits. This does not affect the quadratic convergence of E.

6. Conclusion

The numerical implementation of QLM has been generalized and shown to work in an extremely singular setting. This makes it practically independent of the form of singularity. It yields quadratically convergent energies E and radial solutions $u(x)$ as precise as the numerical integration error and number representation permit, except that $u(x)$ converges geometrically like the Picard algorithm in small, self-adjusting minorization intervals around singularities; it is QLM which assures this convergence at all, and it does not affect E.

The function f_m can be obtained from some representation $\tilde{u}$ of the local nonanalytic solution at the singularity; due to the way the Riccati solution $u(x)$ is defined, simply omitting the tangent function and continuing f_m by a linear function past the inflection point of $\tilde{u}$ makes it a minorant on the entire interval, alleviating the need for a cutoff radius parameter.

The key to convergence is a nonlinear integration point distribution for singular potentials which makes points denser approximately in inverse proportion to radial solution magnitude, thus being able to bridge the small scale of the spike and the large scale of the harmonic term without variable transformation. It is ensured the points form a monotonically increasing sequence. A uniform integration point distribution is used for regular potentials. A Runge–Kutta solver was used to minimize the effect of errors contained in the minorized, or clamped values from the previous iteration it uses. Only four QLM iterations sufficed to get E to 20 digit precision, which is actually less than for regular potentials using equidistant points [18,19]. The same program can be used for both regular and singular potentials.

Acknowledgements

I greatly appreciate discussions with V.B. Mandelzweig.

References

[1] V.C. Aguilera-Navarro, G.A. Estévez, R. Guardiola, J. Math. Phys. 31 (1990) 99.
[2] R. Krivec, Comput. Phys. Commun. 183 (2012) 2601.
[3] W. Bühring, J. Math. Phys. 15 (1974) 1451.
[4] W.M. Frank, D.J. Land, R.M. Spector, Rev. Mod. Phys. 43 (1971) 36.
[5] L.C. Detwiler, J.R. Klauder, Phys. Rev. D 11 (1975) 1436.

[6] J.R. Klauder, Acta Phys. Austriaca (Suppl. 11) (1973) 341.
[7] J.R. Klauder, Phys. Lett. B 47 (1973) 523.
[8] J.R. Klauder, Science 199 (1978) 735.
[9] H. Ezawa, J.R. Klauder, L.A. Shepp, J. Math. Phys. 16 (1975) 783.
[10] B. Simon, J. Funct. Anal. 14 (1973) 295.
[11] E. Buendía, F.J. Gálvez, A. Puertas, J. Phys. A: Math. Gen. 28 (1995) 6731.
[12] F.J. Gómez, J. Sesma, J. Phys. A: Math. Theor. 43 (2010) 385302.
[13] J.P. Killingbeck, G. Jolicard, A. Grosjean, J. Phys. A: Math. Gen. 34 (2001) L367.
[14] R. Krivec, V.B. Mandelzweig, Comput. Phys. Commun. 179 (2008) 865.
[15] V.B. Mandelzweig, J. Math. Phys. 40 (1999) 6266.
[16] R.E. Bellman, R.E. Kalaba, Quasilinearization and Nonlinear Boundary-Value Problems, Elsevier Publishing Company, New York, 1965.
[17] R. Krivec, V.B. Mandelzweig, F. Tabakin, Few-Body Syst. 34 (2004) 57.
[18] R. Krivec, V.B. Mandelzweig, Comput. Phys. Commun. 174 (2006) 119.
[19] R. Krivec, V.B. Mandelzweig, Phys. Lett. A 337 (2005) 354.
[20] R.E. Langer, Phys. Rev. 51 (1937) 669.
[21] R. Krivec, V.B. Mandelzweig, Comput. Phys. Commun. 152 (2003) 165.
[22] W. Herbst, B. Simon, Phys. Lett. B 78 (1978) 304.
[23] W.M. Frank, D.J. Land, J. Math. Phys. 11 (1970) 2014.
[24] P. Calogero, M. Cassandro, Nuovo Cimento 37 (1965) 760.